Measurements of Tilt and Focus for Sodium Beacon Adaptive Optics on the Starfire 3.5 Meter Telescope

Robert Johnson
AFRL/RDS
James Brown
SAIC
James Spinhirne
The Boeing Company

Air Force Research Laboratory, Directed Energy Directorate
3550 Abderdeen Ave. SE, Kirtland Air Force Base, NM, 87117

Abstract: Telescopes with adaptive optics systems can measure high-order aberrations using an artificial laser beacon without the need for a relatively bright object near the object being imaged. Unfortunately, tilt and focus measurements are difficult to obtain from a laser beacon. One solution is to use light from the object being imaged to measure tilt and focus. We characterize the performance of a Shack-Hartmann wavefront sensor with 2×2 sub-apertures for measuring tilt and focus. Specifically, we implemented this scheme for the sodium beacon adaptive optics upgrade to the Starfire Optical Range (SOR) 3.5 meter telescope [1]. We use a wave-optics simulation to predict the performance of the tilt and focus sensor in the SOR sodium beacon system, and compare the results to laboratory measurements.

1. INTRODUCTION

When employing a sodium laser beacon in an adaptive optics system, one can not obtain an absolute measurement of tilt or focus from the beacon to correct images of an object above the Earth's atmosphere. Tilt from the beacon can not be used, because the tilt on the outgoing path is not the same as the tilt on the incoming path. This is often due to jitter on the outgoing beam caused by vibration in the telescope. Absolute focus from the beacon can not be obtained, because the altitude of the sodium layer varies spatially and temporally. In addition, when imaging an Earth-orbiting satellite from a land-based telescope, the range to the satellite varies with telescope elevation angle and hence with time. One can, however, use the beacon for measuring relatively fast focus changes introduced by atmospheric turbulence.

One solution to this dilemma is to use light from the object itself to measure tilt and focus, as in the Keck adaptive optics system [2]. We chose a similar approach for our recent upgrade of the Starfire Optical Range (SOR) 3.5 meter telescope sodium guide-star adaptive optics system. A small amount of the light from the object is redirected from the imaging optical path to a small Shack-Hartmann wavefront sensor with 2×2 subapertures. We use this device, called the tilt and focus sensor, to provide an absolute measure of tilt and focus for the object.

In this paper, we discuss our optical and sensor design and include a brief description of a wave-optics simulation of the tilt and focus sensor. We used the simulation to explore the range of measurement for tilt and focus, cross-coupling of measurements, and errors in measurements in the presence of noise. We then repeated these tests in the telescope coudé laboratory. These simulation and laboratory results do not include atmospheric turbulence effects.

2. FOCUS MEASUREMENT AND CONTROL APPROACH

In the SOR 3.5 meter telescope sodium guide-star adaptive optics system, focus measured from the beacon is used for high-bandwidth focus correction, while focus measured from the object is used for low-bandwidth focus correction. This concept is illustrated in Figure 1. The amount of focus sensed by the sodium beacon wavefront sensor includes

high-bandwidth focus errors introduced by the atmosphere, and low-bandwidth focus errors introduced by changes in range to the sodium layer.

Measurements from the tilt and focus sensor are used to drive a fast steering mirror to control overall wavefront tilt. In addition, tilt and focus sensor measurements are used to drive a linear translation stage that is part of an optical trombone upstream of the sodium beacon wavefront sensor. The purpose of this stage is to adjust for the difference in focus between the object and the sodium beacon. Movement of this stage causes focus to be sensed by the sodium beacon wavefront sensor, which drives the deformable mirror to correct this focus. Range changes due to changes in telescope elevation are added to the trombone commands in open-loop. Also, large amounts of focus are corrected by moving the secondary mirror of the telescope in a very low-bandwidth correction loop. In other words, focus is off-loaded from the deformable mirror to the secondary mirror.

To help understand how this arrangement works, imagine that all control loops are closed, there is no focus sensed by either the sodium beacon wavefront sensor or the tilt and focus sensor, and the deformable mirror is adjusted to provide zero focus. Then imagine there is a small change in range to the sodium layer. This causes focus to be sensed by the sodium beacon wavefront sensor which commands the deformable mirror to remove this focus. This, in turn, causes a focus error to be sensed by the tilt and focus sensor, which is observing light from the object. The tilt and focus sensor drives the optical trombone to introduce the right amount of focus into the sodium beacon wavefront sensor path to cause the deformable mirror to null the focus observed by the tilt and focus sensor. The net result is the sodium beacon wavefront sensor and tilt and focus sensor observe no focus error, the deformable mirror has zero focus applied and the optical trombone has been adjusted to account for the small change in range to the sodium layer.

This convoluted arrangement allows the system to be used for both laser beacon and natural guide star operation. This approach, and a more complicated approach, are described in detail by Link and Foucault [3]. They show these two approaches to focus control have comparable performance in the presence of atmospheric turbulence.

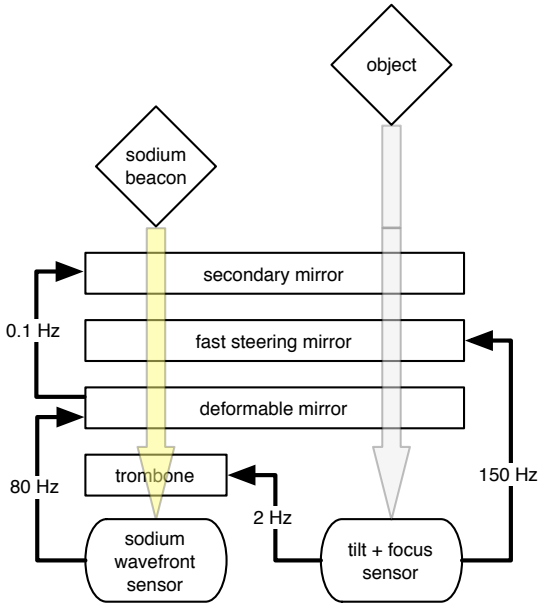

Fig. 1. Focus measurement and control scheme. The frequencies shown are the closed-loop bandwidth of the control systems.

3. Simulation using a Wave Optics Model

To simulate the performance of the tilt and focus sensor, we built a wave-optics model using wave optics techniques outlined in Goodman [4], which were applied to a Shack-Hartmann wavefront sensor by Roggemann and Schulz [5]. The model first maps the phase at the telescope pupil to a lenslet array. The amplitude transfer function of the lenslet array is generated and is used to compute the field just after the lenslet array. This field is then propagated to a multi-element detector at the image plane of the lenslets. From this field, the intensity is calculated and binned to represent photoelectrons as sensed by the individual detector array elements or pixels. Shot noise and read noise are then added.

Since we are interested in measuring tilt and focus, we generated a simple least-squares modal reconstructor to extract the first three Zernike terms, excluding piston, from the simulated detector output [6]. The parameters used as inputs to the model are listed in Table 1. The optical design also includes two sets of optics, one that relays the image of the telescope pupil to the lenslet array, and another that relays the Shack-Hartmann spots formed by the lenslets to a detector array.

Table 1. Key parameters for the tilt focus sensor.

Parameter	Value
wavelength	$0.48-0.64$ μm
lenslet focal length	12.1 mm
lenslet width	1.0 mm
spot relay magnification	0.192
pixel width (binned 2×2)	48 μm
pixels per subaperture	4×4
read noise	5.3 e^-

4. DETECTOR ARRAY

We considered both charge-coupled devices (CCDs) and MIT Lincoln Laboratory geiger-mode avalanche photo diode (APD) arrays for the tilt and focus sensor. Compared to CCDs, APD array technology is less mature, but has the potential to offer vast improvements by eliminating read noise and reducing read-out latency ten-fold [7]. These improvements comes at a cost. APD arrays suffer from effects not inherent in CCDs. In an APD, the probability of a photoelectron causing an avalanche is typically 0.5. In effect, this reduces the quantum efficiency in converting photons to photoelectrons. Also, when a photoelectron causes an avalanche, another photon can be generated, which may cause an avalanche in a neighboring pixel in the quad-cell. This phenomenon is called crosstalk. Finally, APDs must be reset or quenched after an avalanche, before they can detect another photon. A polling circuit periodically checks if an APD has fired; if it has fired, the APD is reset. This leads to a varying dead time during which a photon can not be detected.

In other words, APD arrays promise reduced read-out latency and zero read noise, and with sufficiently weak signals, dead time is not an issue. However, crosstalk can introduce errors computing centroids in quad-cells. Before we built the tilt and focus sensor, the problem of crosstalk had not been solved, so we chose to use a CCD to allow MIT Lincoln Laboratory time to improve APD array performance. Since then, they have reduced crosstalk to under two percent by using metal channel stops between pixels in a quad-cell. The issue of inefficient quenching still remains to be resolved, but it is being addressed with new devices.

For the interim, we chose an e2v CCD39 with SciMeasure electronics for the tilt and focus sensor detector array. The CCD39 is a 80×80 pixel frame-transfer CCD with four output ports. We typically operate the camera at 2000 frames per second with 2×2 pixel binning. Using the photon transfer curve method, we measured the read noise at 7.3 electrons and the digitization gain at 0.46 electrons per count. On the advice of SciMeasure, we have since added shielding to the analog cables, which should reduce the read noise by 2 to 3 electrons, although this has yet to be measured directly. As shown in Figure 2, we measured the average quantum efficiency of the device at 0.9 over the wavelengths of interest, $0.48-0.64$ μm. We also measured the pixel edge diffusion length as 3.6 μm. We did this by scanning a small 6 μm spot across a quad-cell intersection and measuring the response. We then applied the method devised by Tyler [8] to estimate the pixel edge diffusion length.

5. MODEL RESULTS, LAB RESULTS, AND ANALYSIS

Here we compare the modeled performance of the tilt and focus sensor to measurements made in the telescope coudé laboratory. A detailed description and results from modeling a notional tilt and focus sensor are described in our previous paper [9].

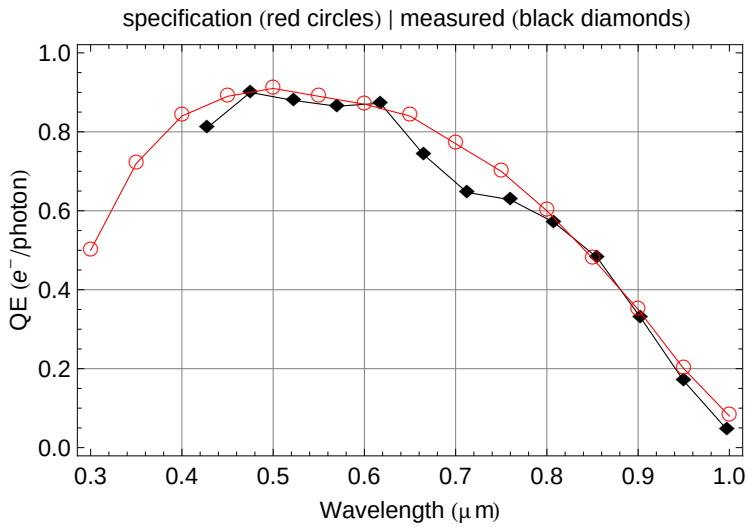

Fig. 2. Specified and measured quantum efficiency of the CCD39.

First, we explored the performance of the sensor by inserting known amounts of tilt and focus into the model and applying a least-squares modal reconstructor. Similarly, in the laboratory, we introduced known amounts of tilt and focus, then recorded the output of the sensor. In the model, we introduced no detector noise, while in the laboratory, we increased the signal so the measurement was dominated by shot noise, making read noise relatively insignificant. For the laboratory measurements, we calibrated the output of the sensor using scaling derived from the optical prescription and the calibrated response of the fast steering mirror for tilt, and the deformable mirror for focus.

For the tilt measurement, the fast steering mirror was scanned in both the vertical and horizontal directions while we collected gradients from the tilt and focus sensor. The light source was a single-mode optical fiber placed conjugate to the focus of the telescope. Figure 3 shows the modeled and the measured response of the sensor to horizontal tilt. Here, the units are microns of RMS wavefront.

Nearly identical results were obtained for vertical tilt, however, the slope of the transfer curve was about three percent less than the slope for horizontal tilt. This might be due to the increased pixel edge diffusion we observed in the vertical direction (column or parallel direction on the CCD) versus the horizontal direction (row or serial direction on the CCD). For both the horizontal and vertical tilt scans, the measured transfer curve slope was slightly less than in the model; this is probably caused by pixel edge diffusion in the CCD.

Figure 4 shows a similar plot for focus. For this measurement, we introduced focus by commanding a static figure onto the deformable mirror. The response of the deformable mirror had been carefully calibrated using a phase-shifting interferometer. For this test, the tilt control loop was closed with a gain of 1.0 times the design gain to help reduce the effect of turbulence in the laboratory. The turbulence in the laboratory made the focus measurement quite variable. In spite of the turbulence, the sensor measured the focus introduced by the deformable mirror reasonably well, with a transfer curve slope slightly less than the modeled slope.

Next, we examined the performance of the tilt and focus sensor in the presence of noise. We repeated the measurements described above, but over a wide range of signal levels and with zero introduced tilt or focus. For this test, we closed the tilt control loop with a gain of 0.01 times the design gain to help keep the Shack-Hartmann spots near the center of the quad-cells and thus where the sensor is most sensitive.

Figure 5 compares the measured tilt error to the modeled tilt error as a function of the total signal detected by the 16 pixels of the sensor. The tilt measurement error decreases rapidly up to about 1000 electrons of signal, then it decreases more slowly. Our laboratory measurements match the modeled results quite well. As shown in our previous paper [9], at low signal levels, read noise is the dominant cause of measurement error and a simple quad-cell out-performs the four sub-aperture Shack-Hartmann sensor. At higher signal levels, where shot noise is the dominant source of measurement error, the four sub-aperture Shack-Hartmann sensor is superior in measuring tilt.

For a 12th visual magnitude object, we expect about 400 electrons total to be detected if the sensor integrates for 0.5

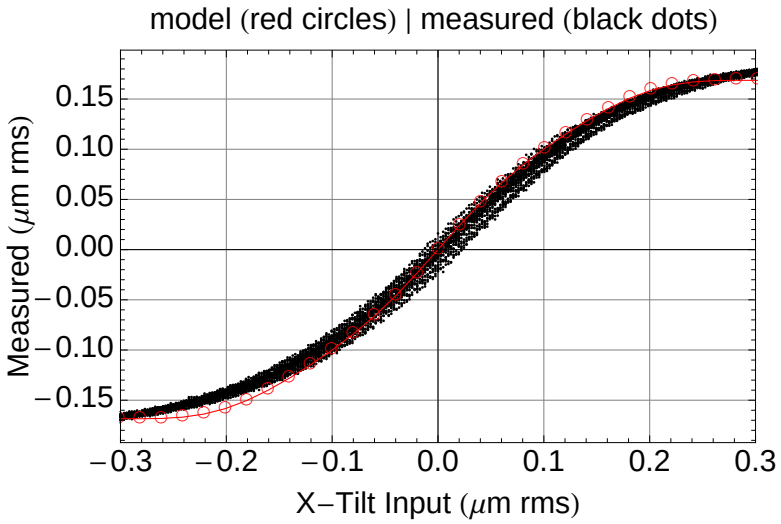

Fig. 3. Tilt transfer function.

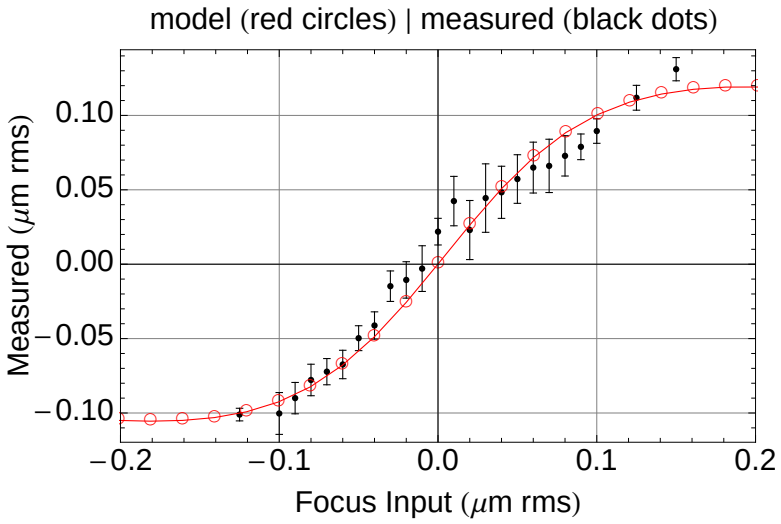

Fig. 4. Focus transfer function.

milliseconds, which corresponds to 2000 frames per second. This assumes a wavelength range of 0.48 to 0.64 microns with a notch at 0.589 microns of 0.02 microns in width. The average optical transmission in this band is about 0.5 and the sensor quantum efficiency is 0.9.

Finally, we measured the focus error as a function of total detected signal, as shown in Figure 6. Because the focus measurement was affected by turbulence in the laboratory, as illustrated in Figure 7, we filtered the focus measurement using a high-pass filter with a 5 Hz cutoff frequency before calculating the RMS focus error, as shown in Figure 8. As with tilt measurement error, the focus measurement error decreases rapidly up to about 1000 electrons, then it decreases more slowly as the signal on the detector is increased. Unlike the tilt measurement error, the focus measurement error is greater than the error predicted by the model.

In summary, the measured transfer functions for tilt and focus match the model predictions well. The tilt measurement error as a function of detected signal agrees well with the model, however, this is not the case for focus measurement error. We will investigate this discrepancy in the future. We expect performance in the presence of low signals will improve when we replace the CCD with an APD array.

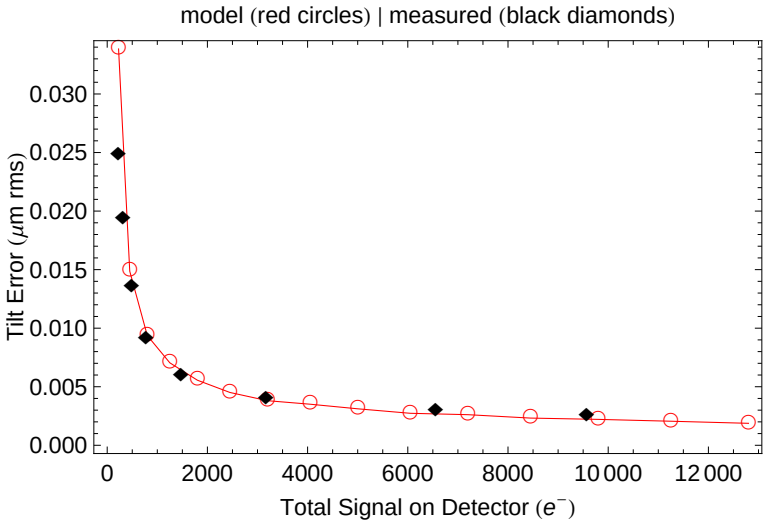

Fig. 5. Tilt error versus signal.

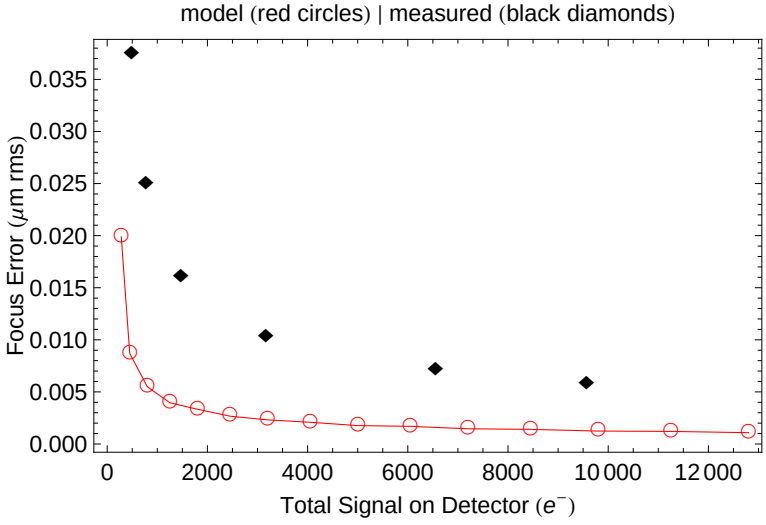

Fig. 6. Focus error versus signal.

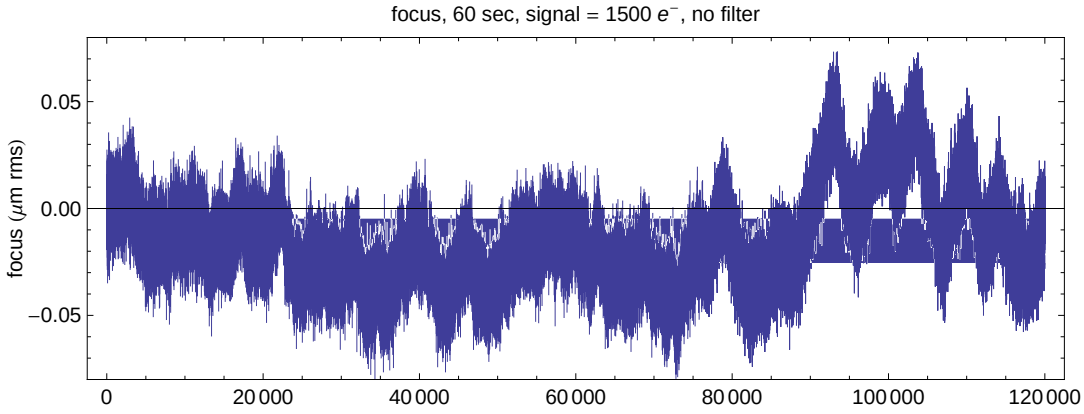

Fig. 7. Focus measurement over a period of 60 seconds.

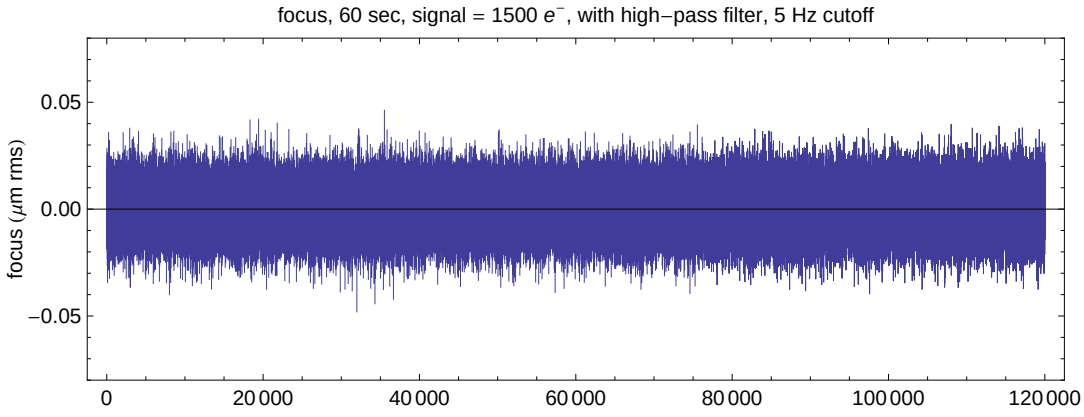

Fig. 8. Focus measurement over a period of 60 seconds, after filtering with a high-pass filter with a 5 Hz cutoff.

6. ACKNOWLEDGMENTS

The authors wish to thank John Wynia for calibrating the deformable mirror and collecting characterization data for the CCD39, Charlie Bleau of SciMeasure for building and programming the CCD39 camera, Mark Eickhoff and Kendrick Walter for installing and aligning the optics, and Gregory Brittelle for writing the tracker interface software.

References

1. Johnson R., Montera D., Schneeberger T., and Spinhirne J., "A New Sodium Guidestar Adaptive Optics System for the Starfire Optical Range 3.5 m Telescope," in *Adaptive Optics: Methods, Analysis and Applications,* Optical Society of America, 2009.
2. Summers D. et al, "Focus and pointing adjustments necessary for laser guide star adaptive optics at the W. M. Keck Observatory," SPIE Astronomical Telescopes and Instrumentation Conference, Glasgow, Scotland, 21–25 June 2004.
3. Link D. and Foucault B., "Investigation of focus control for NGAS," Starfire Optical Range internal memo, 8 May 2007.
4. Goodman J., Introduction to Fourier Optics, McGraw-Hill, New York, 2nd ed., 1996.
5. Roggemann M. and Schulz T., "Algorithm to increase the largest aberration that can be reconstructed from Hartmann sensor measurements," Appl. Opt. 37, pp. 4321–4329, 1998.
6. Noll R., "Zernike ploynomials and atmospheric turbulence," J. Opt. Soc. Am., 66, pp. 207–211, 1976.
7. Aull B. et al, "Geiger-mode quad-cell array for adaptive optics," in *Conference on Lasers and Electro-Optics/Quantum Electronics and Laser Science Conference and Photonic Applications Systems Technologies*, Optical Society of America, 2008.
8. Tyler G., "Accommodation of LITE camera issues by controlling quad-cell optics," The Optical Sciences Company, Report No. TR-1804, October 2009.
9. Johnson R., "Measuring tilt and focus for sodium beacon adaptive optics on the Starfire 3.5 meter telescope," in *Proceedings of the Advanced Maui Optical and Space Surveillance Technologies Conference*, 2008.